Geochemistry Geophysics Geosystems G3

Article
Volume 14, Number 12
6 December 2013
doi: 10.1002/2013GC004950
ISSN: 1525-2027

Published by AGU and the Geochemical Society

The origin of magnetic remanence in stalagmites: Observations from electron microscopy and rock magnetism

B. E. Strauss
Department of Earth Sciences, Institute for Rock Magnetism, University of Minnesota, Minneapolis, Minnesota, USA

J. H. Strehlau
Department of Chemistry, University of Minnesota, Minneapolis, Minnesota, USA

I. Lascu
Department of Earth Sciences, Institute for Rock Magnetism, University of Minnesota, Minneapolis, Minnesota, USA

Now at the Department of Earth Sciences, University of Cambridge, Cambridge, UK

J. A. Dorale
Department of Earth and Environmental Sciences, University of Iowa, Iowa City, Iowa, USA

R. L. Penn
Department of Chemistry, University of Minnesota, Minneapolis, Minnesota, USA

J. M. Feinberg
Department of Earth Sciences, Institute for Rock Magnetism, University of Minnesota, 310 Pillsbury Dr. SE, Minneapolis, Minnesota, 55455, USA (feinberg@umn.edu)

[1] Speleothems, especially stalagmites, hold great potential as recorders of the Earth's ancient magnetic field. However, our understanding of the magnetic mineral assemblages within speleothems is not well developed. We present tandem rock magnetic characterization of bulk samples and electron microscopy of magnetic extracts from five North American stalagmites. Magnetite and goethite are present in all samples, albeit in varying abundances and morphologies. Magnetite grains are likely detrital, showing evidence of transport and weathering, including plumose markings and etch pits. These grains are unlikely to have precipitated abiotically in the cave environment. Titanomagnetite and exsolved intergrowths of Fe-Ti oxides indicate that a significant portion of the magnetic mineral assemblage is allochthonous and was transported into the caves. These Ti-rich grains display a range of morphologies from euhedral to well rounded, indicating that earlier morphological models for speleothem magnetization do not apply in all geologic settings. Goethite was observed in three morphologies: isolated needles, needle aggregates, and polycrystalline aggregates of randomly oriented nanoscale grains. The magnetite and titanomagnetite, as well as their partially oxidized equivalents, likely hold a depositional remanent magnetization (DRM), whereas if goethite grains were precipitated in situ on the stalagmite drip surface, they are more likely to hold a chemical remanent magnetization (CRM) because of their small size and low saturation magnetization. Until the remanence of goethite can be shown to be paleomagnetically meaningful, we propose that paleomagnetic studies of speleothems include a 150°C thermal demagnetization step to remove any goethite remanence.

Components: 10,672 words, 9 figures, 2 tables.

Keywords: speleothem; stalagmite; rock magnetism; electron microscopy; paleomagnetism; environmental magnetism.

Index Terms: 1540 Rock and mineral magnetism: Geomagnetism and Paleomagnetism; 1519 Magnetic mineralogy and petrology: Geomagnetism and Paleomagnetism; 1512 Environmental magnetism: Geomagnetism and Paleomagnetism; 4958 Speleothems: Paleoceanography; 3675 Sedimentary petrology: Mineralogy and Petrology.

Received 23 July 2013; **Revised** 21 October 2013; **Accepted** 23 October 2013; **Published** 6 December 2013.

Strauss, B. E., J. H. Strehlau, I. Lascu, J. A. Dorale, R. L. Penn, and J. M. Feinberg (2013), The origin of magnetic remanence in stalagmites: Observations from electron microscopy and rock magnetism, *Geochem. Geophys. Geosyst.*, *14*, 5006–5025, doi:10.1002/2013GC004950.

1. Introduction

[2] Speleothems, including stalagmites, stalactites, and flowstones, are secondary mineral deposits that form in caves and record valuable information about the environment in which they grow [*Fairchild et al*., 2007]. Speleothems were first proposed as paleomagnetic recorders in the 1970s, when *Latham et al*. [1979] measured the ancient geomagnetic field directions recorded by a group of flowstones and stalagmites and established that speleothems can hold stable magnetizations for thousands of years after their initial deposition in pre-existing caves. Throughout the 1980s, Latham used speleothems to construct secular variation curves that aligned well with data collected from sediment cores and archaeological material [*Latham et al*., 1982, 1986, 1989]. This work sparked a series of paleomagnetic studies expanding on his theories over the next two decades [e.g., *Morinaga et al*., 1986, 1987, 1992; *Perkins and Maher*, 1993; *Perkins*, 1996; *Openshaw et al*., 1997]. *Perkins* [1996] was the first to perform electron microscopy on magnetic extracts from speleothems, providing independent confirmation of magnetic results and giving unprecedented insight into the processes involved in remanence acquisition in stalagmites and flowstones.

[3] The major obstacle for most paleomagnetic studies on speleothems is the low magnetic intensity displayed by stalagmites and flowstones, with natural remanent magnetization (NRM) intensities typically ranging from 10^{-6} to 10^{-3} Am^{-1} [see *Latham et al*., 1982, 1986, 1989; *Perkins and Maher*, 1993; *Perkins*, 1996]. The equivalent magnetization for a 2 cm cube (8 cm^3) would range from 8×10^{-12} to 8×10^{-9} Am^2, which is close to the sensitivity limit for most SQUID-based cryogenic rock magnetometers (10^{-12} to 10^{-11} Am^2). In this regard, the challenges for paleomagnetic studies on "clean" speleothems (i.e., those devoid of flood material) are similar to those faced by studies on pelagic limestones with very little detrital input, where weak NRM intensities make the acquisition of progressive demagnetization data difficult. To overcome the difficulties presented by such weak magnetizations, researchers typically rely on large sample volumes ($\geq$8 cm^3) that average geomagnetic field behavior on timescales of 100–4000 years per sample [e.g., *Osete et al*., 2012].

[4] In recent years, improved magnetometer sensitivities have enabled the measurement of ever-smaller samples of stalagmites and flowstones, thereby refining the potential temporal resolution of speleothem paleomagnetic records [e.g., *Lascu and Feinberg*, 2011; *Osete et al*., 2012; J. M. Feinberg et al., Magnetically derived flood recurrence rate estimates from stalagmites in southeastern Minnesota, submitted to, 2013]. As continuous recorders in which lock-in time is subannual and material suffering from postdepositional alteration is readily identified and avoided [*Lascu and Feinberg*, 2011], speleothems are an attractive alternative to materials like the lava flows and sediment cores more commonly used in paleomagnetic research. However, the mechanisms of remanence acquisition in speleothems are still poorly understood, and paleomagnetic results currently cannot be evaluated with respect to their origins.

[5] Most speleothems are formed when calcite ($CaCO_3$) precipitates from carbonate-rich groundwater as it enters pre-existing caves, producing secondary deposits [*Fairchild et al*., 2007]. Stalagmites grow through the accumulation of calcite on surfaces below drip points, building subannual layers at rates ranging from 5 μm to 300 μm per

year [*Fairchild et al*., 2007]. This calcite is a nearly ideal material for uranium-series dating [*Dorale et al*., 2004], making stalagmites useful tools for paleoclimate research [e.g., *Dorale et al*., 1998; *Vacco et al*., 2005; *Denniston et al*., 2007; *Dasgupta*, 2008; *Oster et al*., 2010]. Many stalagmites display annual laminations, with differential colored bands reflecting seasonal changes in the concentration of humic substances and fulvic acids, as well as detrital grains, present in the stalagmite's source waters [*Lascu and Feinberg*, 2011; *Fairchild et al*., 2007]. Additionally, periodic floods may deposit layers of sediment, which contains a significant fraction of ferromagnetic iron oxides compared to dripwater-formed calcite, on the external surfaces of stalagmites and flowstones [*Lascu and Feinberg*, 2011; *Fairchild et al*., 2007]. Both drip and flood processes can introduce detrital material, which may include magnetic minerals that formed outside of the cave, into a stalagmite or flowstone. After deposition on the drip surface of the speleothem, the magnetization of the ferromagnetic detritus is locked in place by the subsequent precipitation of accumulating calcite.

[6] While the dichotomy between drip water and flood water has been described with respect to calcite precipitation rates and speleothem morphology [*Lascu and Feinberg*, 2011], its implications for rock magnetism are not well defined. In particular, no study has examined whether the presence or absence of flood material in a bulk speleothem sample is reflected in its magnetic mineral assemblage, nor described the corresponding role of authigenic iron oxide precipitates. Further, as researchers continue to examine whether magnetic mineral assemblages in speleothems can be used as proxies for environmental change [e.g., *Osete et al*., 2012], a clearer understanding of the grain sizes, shapes, elemental chemistry, and physical arrangements of iron oxides and oxyhydroxides is needed.

[7] Previous studies of paleomagnetism in stalagmites and flowstones have described the magnetic mineral assemblage in speleothems using observations about the magnetic properties of bulk samples, which serve as proxies for composition and grain size [e.g., *Perkins and Maher*, 1993]. However, this geophysical approach is not sufficient to develop a detailed story of remanence acquisition. Questions about the significance of in situ grain growth and alteration, as well as the effects of flood material in magnetic studies, remain unanswered. Through microscopic study of magnetic extracts, modeled after the pioneering work of *Perkins* [1996] and later *Rusanov et al*. [2000], grain morphology and elemental compositions may be considered, expanding our understanding of the processes involved in the introduction and incorporation of magnetic material in speleothems.

[8] *Perkins* [1996] analyzed magnetic extracts from stalagmites and flowstones from the UK (England and Wales) using scanning electron microscopy and transmission electron microscopy (SEM and TEM) and proposed a remanence acquisition model based largely on the morphology and composition of the observed magnetic mineral assemblage. Three morphological categories were identified: abraded irregular grains, unabraded euhedral grains, and needle-like grains. Perkins suggested that the abraded grains were rounded during stream transport and therefore provided crucial evidence for the presence of detrital magnetic material in speleothems and the corresponding importance of depositional remanent magnetization (DRM). Energy dispersive spectroscopy (EDS) measurements conducted via SEM indicated that a large fraction of these abraded grains contained both iron and titanium, which, when coupled with rock magnetic results revealing the presence of titanomagnetite ($Fe_{3-x}Ti_xO_4$), is consistent with an allochthonous origin. EDS measurements of the euhedral grains showed only iron, indicating that they were nearly pure stoichiometric magnetite (Fe_3O_4). The needle-like grains found in two flowstone samples were too small to be analyzed using EDS, and instead were inferred to be goethite (α-FeO·OH) based on their morphological similarity to authigenic goethite crystals and the magnetic signature of goethite in bulk sample measurements. Perkins speculated that both goethite and magnetite precipitated in situ on a speleothem's drip surface and thus constituted a chemical remanent magnetization (CRM). *Perkins* [1996] thereby demonstrated the value of tandem microscopy and magnetic analyses and laid out a model highlighting the combined roles of DRM and CRM in the acquisition of magnetization in speleothems.

[9] *Rusanov et al*. [2000] employed Mössbauer spectroscopy and SEM-TEM analysis to examine the magnetic mineral assemblage in magnetic extracts from a stalagmite collected from a private cave in the UK, revealing the presence of fine-grained hematite (~20 nm) and superparamagnetic goethite. No evidence of magnetite was found through either analysis. This study confirmed that goethite can occur in stalagmites and demonstrated

that the remanence of some speleothems may be dominated by phases other than magnetite.

[10] Unlike lava flows and sediment cores, which have well-established methodological protocols, speleothems are still a fairly new tool in rock magnetism and best practices have not yet been developed. This study concerns the quantitative characterization of magnetic materials occurring at mass loadings very near the detection limits and the edge of measurability for even the most sensitive of instruments. Through coupled SEM and TEM study of magnetic extracts, we increase the range of grain sizes that may be analyzed and the spectrum of chemical analytic methods available, making it possible to address some of the analytical gaps in *Perkins* [1996]. We also aim to provide basic guidelines for sample selection criteria and characterization methods for future research in speleothem magnetism. An improved understanding of the magnetic mineralogy of speleothems is a critical step toward the establishment of speleothem magnetism as a useful and practical tool for the paleomagnetism and environmental magnetism communities.

2. Methods

2.1. Samples and Setting

[11] This study focuses on five stalagmite samples collected from four caves in the United States. All samples were generously provided by other researchers. Three of the samples were collected from privately owned caves in southeast Minnesota: SVC982 and SVC06 from Spring Valley Caverns [*Dasgupta*, 2008; *Shapiro*, 2007] and NC11-1 from Niagara Cave (C. Alexander, personal communication). Both caves are located in the Driftless Area, a region spanning southeastern Minnesota and western Wisconsin that underwent multiple glaciations but was not covered by ice during the most recent glacial maximum [*Shapiro*, 2007]. As a result, glacial till covers much of the surface above these caves and contains mineral fragments from intrusive and extrusive volcanic rocks that originally formed in northern Minnesota and Canada. Sample CC-99-DBL-L was collected from Crevice Cave, Missouri, which is located in a loess plateau ~200 km south of the most recent glacial maximum ice sheet extent [*Dorale et al.*, 1998]. Sample BCC10 was collected from Buckeye Creek Cave, West Virginia, which is situated in the Allegheny Mountains [*Hardt*, 2010]. Two of these stalagmites (NC11-1, SVC982) are known to include flood layers [*Dasgupta*, 2008; C. Alexander, personal communication] and two (SVC06, BCC10) are composed of clean laminated calcite with no indication of flooding (E. C. Alexander, personal communication [2012]; R. L. Edwards, personal communication [2011]). The fifth (CC-99-DBL-L) was collected from an area of Crevice Cave where multiple stalagmites have been shown to contain flood layers, but flood layers have not been conclusively identified in this sample.

2.2. Rock Magnetic Characterization

[12] All magnetic measurements were conducted at the Institute for Rock Magnetism at the University of Minnesota, using bulk stalagmite samples (~0.5 cm^3 chips). While magnetic extracts (described below) are able to provide a representative sampling of the varieties of magnetic minerals present in each speleothem, the extraction process may have inherent collection biases that do not accurately capture the relative abundances of magnetic minerals present within each sample. Rock magnetic measurements on bulk samples should provide a clearer picture of which mineral phases dominate the magnetic remanence held by a given sample.

[13] Room-temperature hysteresis experiments were conducted on a Princeton Measurements Vibrating Sample Magnetometer with a nominal sensitivity of 10^{-9} Am^2. Major hysteresis loops and backfield curves were collected for chips of each speleothem. Low-temperature experiments were conducted on two Quantum Designs Magnetic Property Measurement System (MPMS) cryogenic magnetometers with nominal sensitivities of 10^{-10} Am^2. A variety of low-temperature measurements were conducted, each following one of three protocols:

[14] 1. In a Field Cooled-Zero Field Cooled (FC-ZFC) experiment, each subsample was cooled from room temperature to 10 K, first in a 2.5 T field and then in zero field, and given a 2.5 T isothermal remanent magnetization (IRM). Magnetization was measured during warming back to room temperature in zero field. These measurements enable the identification of diagnostic magnetic mineral transitions and help to determine the dominance of either multidomain (ZFC > FC below 120 K) or single-domain (FC > ZFC below 120 K) grains in the magnetic mineral assemblage.

[15] 2. During the low-temperature cycling of a room-temperature saturation isothermal remanent magnetization (RTSIRM), a 2.5 T IRM was

imparted to each subsample at room temperature; magnetization was then measured during cooling to 10 K and subsequent warming to 300 K, both in zero field. Like FC-ZFC measurements, RTSIRM measurements may be used in the identification of magnetic mineral compositions and multidomain to single-domain ratios, and are one of the most sensitive indicators for the presence of pure stoichiometric magnetite.

[16] 3. The frequency dependence of magnetic susceptibility was measured for one subsample from each stalagmite using a field of 0.3 mT at frequencies of 1, 6, 32, 178, and 997 Hz. These measurements are critical for the detection of superparamagnetic grains.

[17] Demagnetization of remanent magnetizations was conducted on secondary subsamples from each stalagmite using cryogenic magnetometers: either a 2G Enterprises superconducting rock magnetometer (SRM), with a nominal sensitivity of 10^{-11} Am^2, or a 2G Enterprises U-channel magnetometer, with a nominal sensitivity of 10^{-12} Am^2. Each experiment followed a sequence of progressive alternating field (AF) steps until either 95% of the subsample's initial magnetization was removed or the maximum AF demagnetization step was reached.

2.3. Microscopy

[18] Magnetic extracts were prepared using a two-step process. First, the carbonate component of the speleothem was dissolved using a mildly acidic buffer solution. Second, the undissolved residue was resuspended and the resulting mixture subjected to a strong magnetic field following either the methods of *Perkins* [1996] or the alternate method described below, which enabled the further separation of grains according to magnetic moment.

2.3.1. Dissolution

[19] Stalagmite specimens were subsampled with either a bandsaw or a circular saw and carefully sanded by hand to remove any trace metal left by the cutting process, after which subsamples were rinsed, sonicated in water for 180 s, and dried at room temperature. Each group of subsamples (totaling approximately 12–15 g) was then disaggregated into small pieces, as recommended by *Perkins* [1996]. Each sample was additionally ground using a ceramic mortar and pestle until no pieces larger than 1 cm^3 remained.

[20] The dissolution procedure was adapted from *Perkins* [1996]. The buffer solution for dissolution was a 4:1 mixture of 2 M CH_3COOH (Mallinckrodt) and 1 M $NaCH_3COO$ (Aldrich), both prepared using Milli-Q water (Millipore, 18.2 Ω·cm). The crushed stalagmite was added to a 250 mL Erlenmeyer flask and dissolved in 200 mL of buffer solution. The flask was mixed using a Cole Parmer Orbital Shaker 51300 Series set at 162 rotations per minute (rpm) for 7 days. During the dissolution, the pH increased from 4 to approximately 5.5.

[21] After the stalagmite was completely dissolved, the remaining clay and iron oxide residue was collected by transferring the suspension to a centrifuge tube and spinning at 5000 rpm for 3 min using an Eppendorf 5804 centrifuge. The supernatant was decanted and the residue was rinsed three times by adding 40 mL Milli-Q water to the centrifuge tube, shaking for 2 min, spinning at 5000 rpm for 3 min, and decanting. The final residue was dried in air at room temperature.

2.3.2. Magnetic Extraction

[22] Initial extraction was conducted using a peristaltic pump, after the methods of *Perkins* [1996]. The residue was resuspended in 10 mL of Milli-Q water, to which 0.2 mL of 10% $(NaPO_3)_6$ (Fisher Scientific) was added as a deflocculant. This suspension was then pumped through a vertical loop of plastic tubing past a strong magnet in a plastic sleeve. Extracts were washed from the sleeve into a collection vessel with a stream of distilled deionized water once per day for 7–15 days. This method was somewhat successful for samples with a high concentration of detrital matter; however, its efficiency was decreased substantially by a backup of sediment at joints in the loop of tubing.

[23] Subsequent magnetic extraction was performed in two steps, aimed at separating strongly and weakly magnetic particles for characterization in order to reduce the obscuring effects of magnetic attraction between grains during microscopy. To extract strongly magnetic material, the residue was first added to a 50 mL Erlenmeyer flask containing 30 mL of Milli-Q water. A neodymium magnet was taped approximately 1 cm from the bottom edge, separated from the glass at a fixed distance of 1.7 cm, imposing a field of ~10–16 mT at the wall of the flask. The suspension was agitated using a shaker table set at 105 rpm for 1 h. With the magnet still in place, the suspension was carefully decanted without dislodging the material that had been attracted to the magnet. Once all of the suspension had been decanted, the magnet was removed and the strongly magnetic

material was collected using 1–3 mL of Milli-Q water. To extract weakly magnetic material, the above process was repeated using the same neodymium magnet with the decanted suspension, with the magnet affixed directly to the side of the flask, imposing a field of ~80–290 mT at the wall of the flask.

2.3.3. SEM/TEM

[24] Strongly magnetic particles were characterized using a JEOL 6500 SEM. Samples were prepared for SEM by allowing 1–3 drops of the strongly magnetic material to dry on a 12 mm square of carbon tape (SPI Supplies, Structure Probe, Inc.) without carbon coating. Energy dispersive spectroscopy (EDS) was conducted using a Thermo-Noran Vantage system for elemental analysis. SEM-EDS systems are often calibrated using a "standardless" algorithm; under the best experimental conditions, this algorithm gives absolute elemental concentrations an accuracy of ±5% [*Thermo Electron Corporation*, 2009]. Interpretation of elemental measurements acquired with SEM-EDS in this study relies on elemental ratios (e.g., Fe/O or Fe + Ti/O) rather than absolute concentrations (e.g., [Fe] or [Ti]).

[25] Weakly magnetic particles were characterized using a FEI Tecnai T12 high-resolution TEM (HRTEM) operated at 120 kV and equipped with a LaB_6 electron source. Images and compositional measurements were collected with a Gatan charge-coupled device (CCD) camera and Oxford Model 6767 EDS system, respectively. TEM samples were prepared by placing a drop of the weakly magnetic extract on a 3 mm holey carbon coated copper grid (SPI Supplies). Each droplet was allowed to dry, leaving its residual magnetic extract on the grid, and additional drops were added in the same manner so that the final TEM samples contained the magnetic mineral assemblage from 1–10 drops. Selected area electron diffraction (SAED) patterns were collected for compositional analysis. Spacings and angles were measured in Digital Micrograph (Gatan Inc., V. 3.9.4).

[26] All of the SEM and TEM images shown in this paper are modified only in linear adjustments to brightness and contrast across the image to use the full range of available grayscale values. All microscopy was conducted at the Characterization Facility in the College of Science and Engineering at the University of Minnesota.

3. Results

[27] All samples showed at least one indicator of pure stoichiometric magnetite and goethite, and most displayed a range of magnetic mineral compositions, morphologies, and grain sizes (Table 1).

3.1. Rock Magnetism

[28] Rock magnetic experiments at both low and room temperature revealed a variety of magnetic mineral assemblages (Figure 1 and Table 2). The concentration of magnetic minerals in some samples was sufficiently low to make detection difficult in some cases. Room-temperature hysteresis

Table 1. Summary of Magnetic and Microscopic Results by Sample[a]

Sample	Cave	State	FL	Analysis	Mag	Hem	Gth	TMag	Exs	Spherules
NC11-1	Niagara Cave	MN	Y	Magnetic	Y	N	Y-Trace	Y	Y	Y
				TEM	N	N	Y-Solitary needles			
				SEM	Y	Y[c]	Y-Needle aggregates			
SVC982	Spring Valley Caverns	MN	Y	Magnetic	Y	N	Y	Y	Y	Y
				TEM	N	N	Y-Solitary and polycrystalline aggregate			
				SEM	N	Y[c]	N			
SVC06	Spring Valley Caverns	MN	N	Magnetic	N	N	N	N	N	N
				TEM	N	N	N			
				SEM	N/A	N/A	N/A			
CC-99-DBL-L	Crevice Cave	MO	N[b]	Magnetic	Y	N	Y-Trace	Y	Y	Y
				TEM	N	N	Y-Needle aggregates			
				SEM	N	N	Y-Needle aggregates			
BCC10	Buckeye Creek Cave	WV	N	Magnetic	Trace	N	Y-Abundant	N	N	N
				TEM	N	N	Y-Needle aggregates			
				SEM	N/A	N/A	N/A			

[a]Header abbreviations: flood layers (FL), magnetite (Mag), hematite (Hem), goethite (Gth), titanomagnetite (TMag), exsolution texture (Exs). Y = detected, N = theoretically detectable but not detected, N/A = not applicable.
[b]CC-99-DBL-L has no observable flood layers but was collected in a region of Crevice Cave that experiences flooding.
[c]Hematite detected only as intergrowths with ilmenite. Mineral name abbreviations from *Whitney and Evans* [2010].

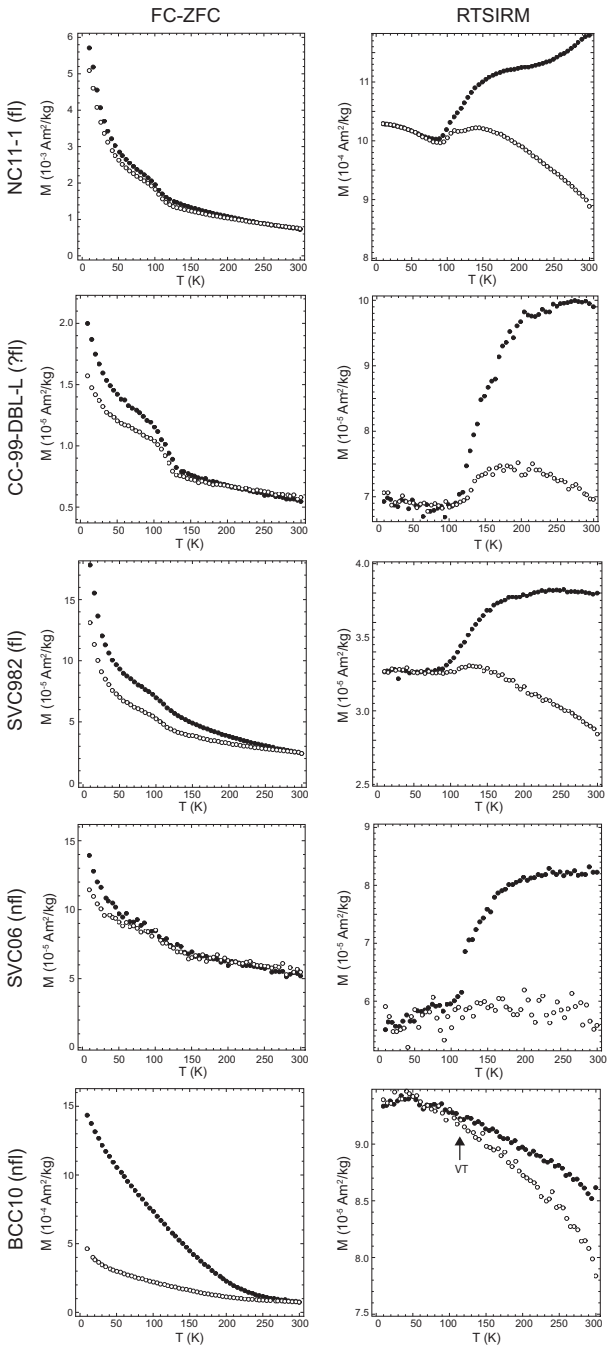

Figure 1. Representative low-temperature MPMS experimental results by sample, with FC-ZFC measurements (filled circles on FC, open circles on ZFC) at left and RTSIRM measurements (filled circles on cooling, open circles on warming) at right. Samples with flood layers indicated by (fl); samples with no flood layers indicated by (nfl). Arrow in RTSIRM for BCC10 indicates Verwey transition (VT).

measurements revealed a small ferromagnetic contribution in all five samples, largely masked by the diamagnetic signal of the host calcite in samples BCC10 and SVC06, which do not contain flood layers. Samples containing flood layers showed a relatively decreased diamagnetic contribution or an added paramagnetic contribution, indicated by a positively sloping high-field magnetic susceptibility.

[29] Analysis of secondary electron images collected in SEM revealed a broad range of grain sizes at the submicron to micron scale, with a broad distribution of grains between 0.1 μm and 10 μm in diameter and outliers ranging up to 300 μm.

[30] The five stalagmites may be ranked in order of their mass normalized magnetic moment, though the parameters used to derive this ranking greatly impact its adherence to the working model of speleothems with flood layers (fl) as "magnetically stronger" and speleothems without flood layers (nfl) as "magnetically weaker," a dichotomy that may be better described as a spectrum. According to mass normalized saturation magnetization (Ms), which is primarily a function of the concentration of magnetic material in a bulk sample:

[31] NC11-1 (fl) >> SVC06 (nfl) ~ SVC982 (fl) > BCC10 (nfl) > CC-99-DBL-L (?fl)

[32] However, according to room-temperature saturation isothermal remanent magnetization (RTSIRM), which is a sensitive indicator of magnetic grain size distribution:

[33] NC11-1 (fl) >> BCC10 (nfl) > SVC982 (fl) ~ SVC06 (nfl) > CC-99-DBL-L (?fl)

[34] Thus, the presence or absence of flood layers in a stalagmite is not necessarily indicative of the intensity of its magnetization; other factors must also be considered.

[35] Five major groups of magnetic minerals were identified using a combination of rock magnetic and electron microscopic techniques, including magnetite, titanomagnetite, goethite, exsolved grains, and spherules. Details for each subgroup are reported below.

3.2. Magnetite

[36] Both rock magnetic measurements and electron microscopy indicate the presence of pure stoichiometric magnetite in all five samples. RTSIRM and FC-ZFC experiments show a decrease in magnetization at ~120 K, characteristic of the Verwey crystallographic transition in magnetite (Figure 1). In sample BCC10, the contribution from goethite was sufficiently large to mute the Verwey

Table 2. Rock Magnetic Results by Sample[a]

				Hysteresis Parameters					MPMS Parameters			
Sample	Cave	State	FL	Ms (Am^2/kg)	Mr (Am^2/kg)	Bc (mT)	Bcr (mT)	RTSIRM (Am^2/kg)	χfd%	Verwey	Morin	Goethite
NC11-1	Niagara Cave	MN	Y	1.38×10^{-2}	1.12×10^{-3}	9.4	44.3	1.27×10^{-3}	< 0.0%	Y	N	Y
SVC982	Spring Valley Caverns	MN	Y	4.37×10^{-4}	6.09×10^{-5}	10.5	35	5.80×10^{-5}	−4.4%	Y	N	Y
SVC06	Spring Valley Caverns	MN	N	4.80×10^{-4}	1.41×10^{-5}	6.4	42.3	5.57×10^{-5}	< 0.0%	Y (RTSIRM)	N	N
CC-99-DBL-L	Crevice Cave	MO	N[b]	6.19×10^{-5}	6.19×10^{-5}	18.5	N/A	9.90×10^{-6}	< 0.0%	Y	N	Y
BCC10	Buckeye Creek Cave	WV	N	1.50×10^{-4}	5.60×10^{-5}	19	60.8	6.49×10^{-5}	0.4%	Y (RTSIRM)	N	Y

[a]Header abbreviations: flood layers (FL), saturation magnetization (Ms), saturation remanence (Mr), coercivity (Bc), coercivity of remanence (Bcr), frequency dependence of susceptibility (χfd%, defined as 100 × ((low-frequency susceptibility) − (high-frequency susceptibility))/(low-frequency susceptibility)). Y = detected, N = theoretically detectable but not detected, N/A = not applicable.
[b]CC-99-DBL-L has no observable flood layers but was collected in a region of Crevice Cave that experiences flooding. Susceptibility results reported are based on single measurements. All other quantities reported are averages of multiple mass-normalized measurements.

transition during FC-ZFC experiments, although the transition was detected in RTSIRM results. Similarly, due to very low concentrations of magnetic minerals, all magnetic results for sample SVC06 were extremely noisy, making the Verwey transition more difficult to detect through FC-ZFC experiments than through RTSIRM.

[37] Approximately half of the extracted grains analyzed with SEM-EDS in NC11-1 were identified as magnetite, based on Fe:O ratios of 0.75 and the absence of Ti (Figure 2). Most magnetite grains are rounded and heavily abraded, with some displaying triangular etch pits on relict {111} facets. The surfaces of some grains show shrinkage cracks that are likely associated with the onset of partial oxidation of magnetite to maghemite (γ-Fe_2O_3), during which the resulting decrease in d-spacing leads to a negative volume change (example in Figure 2d). A portion of the magnetite grains show freshly fractured surfaces with plumose markings still visible, but without the triangular etch pits and partially oxidized textures that define older, more weathered surfaces on the magnetite grains. We interpret these variable surface textures to have formed during the transport of detrital grains prior to their introduction into the cave.

[38] Pure magnetite was not detected through EDS in other samples, which is most likely the result of sampling bias, as all samples display evidence of the Verwey transition in low-temperature magnetic measurements. These results demonstrate the power of combined rock magnetic and microscopic analyses: although one technique may not fully describe the composition of a given sample, most (if not all) mineral types can be captured through the use of correlative analytical techniques.

3.3. Titanomagnetite

[39] Frequency dependence of susceptibility experiments produced in-phase susceptibility curves consistent with the presence of titanomagnetite of varying compositions [*Moskowitz et al.*, 1998] for samples NC11-1 and SVC982. In magnetic extracts, EDS spectra revealed titanomagnetite grains with compositions ranging from TM02 to TM99, with most values below TM60 and a mean composition of TM38.

[40] Titanomagnetite grain morphology varies widely, ranging from euhedral to heavily abraded, in samples NC11-1, CC-99-DBL-L, and SVC982 (Figure 3). Some titanomagnetite grains show similar surface textures to the magnetite grains observed in sample NC11-1, including triangular

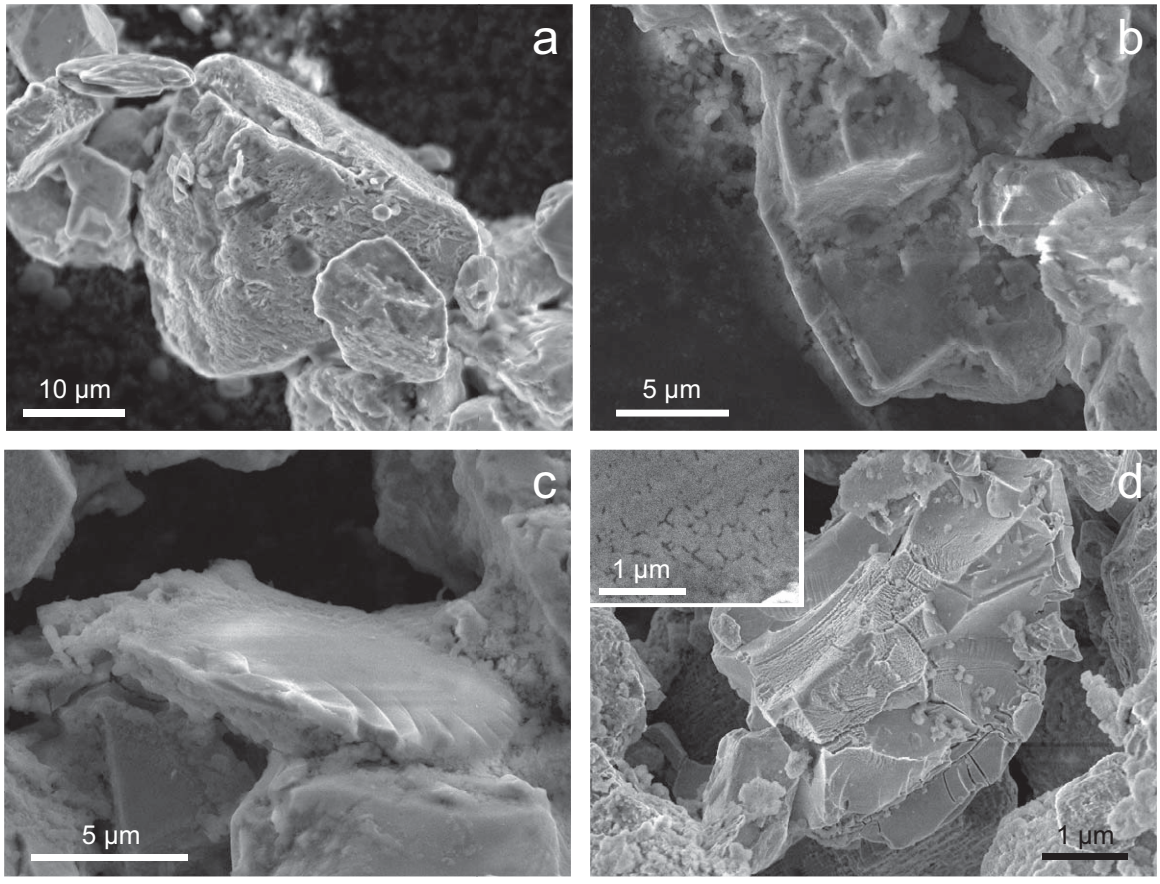

Figure 2. Representative SEM images of magnetite grains, identified by EDS, from sample NC11-1 (fl). (a) Rounded grain with triangular etch pits. (b) Euhedral faceted grain. (c) Irregular grain with plumose texture. (d) Shrinkage cracks, possibly indicating maghemite, from sample CC-99-DBL-L (?fl); inset from sample NC11-1.

etch pits and plumose markings. The euhedral titanomagnetite grains found in this study do not fit into the morphological model of *Perkins* [1996], in which all euhedral grains were thought to be pure magnetite that precipitated either inside the cave or close to the cave system as part of pedogenic magnetic enhancement.

[41] TEM analysis of the weakly magnetic extract yielded no positive identification of magnetite or titanomagnetite, consistent with the expected outcome of the differential magnetic extraction method, during which strongly magnetic material (e.g., magnetite and titanomagnetite) would be isolated in the extract to be studied via SEM.

3.4. Goethite

[42] Rock magnetic evidence for the presence of goethite includes a separation of the FC and ZFC data from 10 K to 300 K and/or a decreasing trend with an increasing temperature in RTSIRM data. The magnetism of sample BCC10 was dominated almost exclusively by goethite, while all other samples included goethite as a secondary magnetic carrier.

[43] Evidence for goethite was found in magnetic extracts from all samples, although the composition of goethite could not be determined during SEM analysis through EDS. Every sample studied under TEM, with the exception of sample SVC06, included goethite, identified by significant Fe in EDS spectra and diffraction analysis of SAED patterns. We categorize observed goethite into three morphological classes: (1) needle aggregates, (2) solitary needles, and (3) polycrystalline aggregates.

[44] Aggregates of goethite needles on top of clay minerals (Figure 4) were found in samples CC-99-DBL-L and BCC10. Individual needles were <1 μm in length and <0.2 μm wide. Both TEM-EDS and electron diffraction patterns collected from needle tips protruding from the edge of the clay mineral host confirm the needle-shaped grains as goethite. A large Fe:Si ratio was detected by

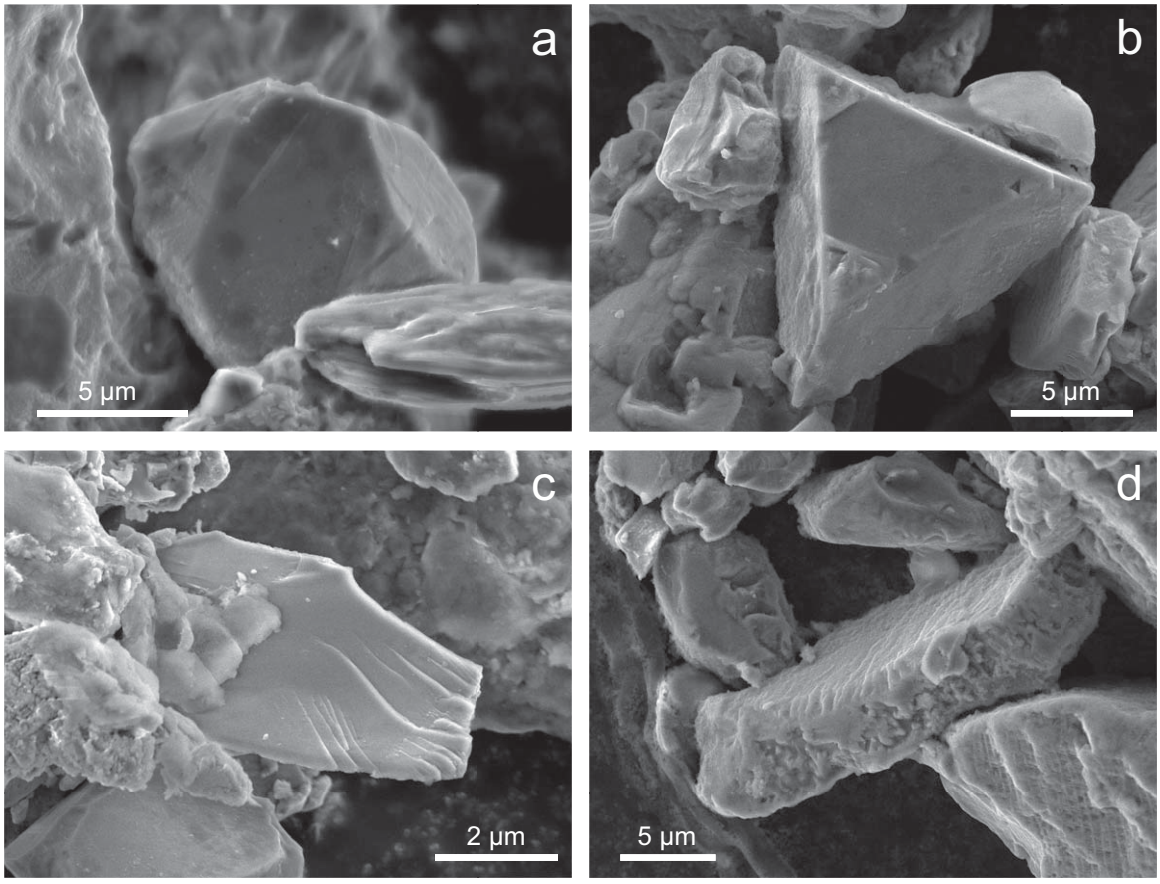

Figure 3. Representative SEM images of titanomagnetite grains, identified by EDS. (a) Euhedral grain from NC11-1 (fl). (b) Euhedral grain with triangular etch pits from NC11-1. (c) Grain with plumose texture from SVC982 (fl). (d) Grain with irregular pitting from NC11-1.

TEM-EDS (the Si is thought to originate from the host mineral), and the measured d-spacings in the SAED pattern match the known values of the (111), (002), and (042) goethite planes. Other iron oxides, including magnetite and hematite, do not consistently correlate to these measured d-spacings, providing further evidence that the identity of the needle-shaped grains is goethite.

[45] Twinned and solitary goethite needles (examples shown in Figure 5) were found in samples NC11-1 and SVC982. Observed twin angles of the goethite needles are consistent with the documented 117.5° twin angle of goethite [*Cornell and Schwertmann*, 2003]. In the case of solitary needles, goethite composition was confirmed by both EDS and SAED, which revealed a high Fe elemental composition and indexed goethite diffraction pattern (Figure 5b).

[46] A polycrystalline aggregate of randomly oriented nanometer-scale goethite crystallites (Figure 6) was found in sample SVC982. EDS spectra of this polycrystalline aggregate particle reveal a primarily iron oxide matrix, with d-spacings in the SAED pattern consistent with polycrystalline goethite. HRTEM of the particle edge confirms its polycrystallinity, displaying ~5 nm islands of goethite with multidirectional lattice fringes that match the expected d-spacing (Figure 6b).

[47] Grains with needle-like morphologies were also observed through SEM in samples NC11-1, SVC982, and CC-99-DBL-L, though these grains were not subject to EDS due to their small size.

3.5. Exsolved Grains

[48] SEM examination of samples NC11-1, SVC982, and CC-99-DBL-L revealed multiple grains featuring exsolution microtextures, with one intergrown phase preferentially etched to reveal networks of exsolved lamellae (Figures 7a–7d). Intergrowths of magnetite and ulvöspinel (Fe_2TiO_4) with lamellae intersecting at 90°, which

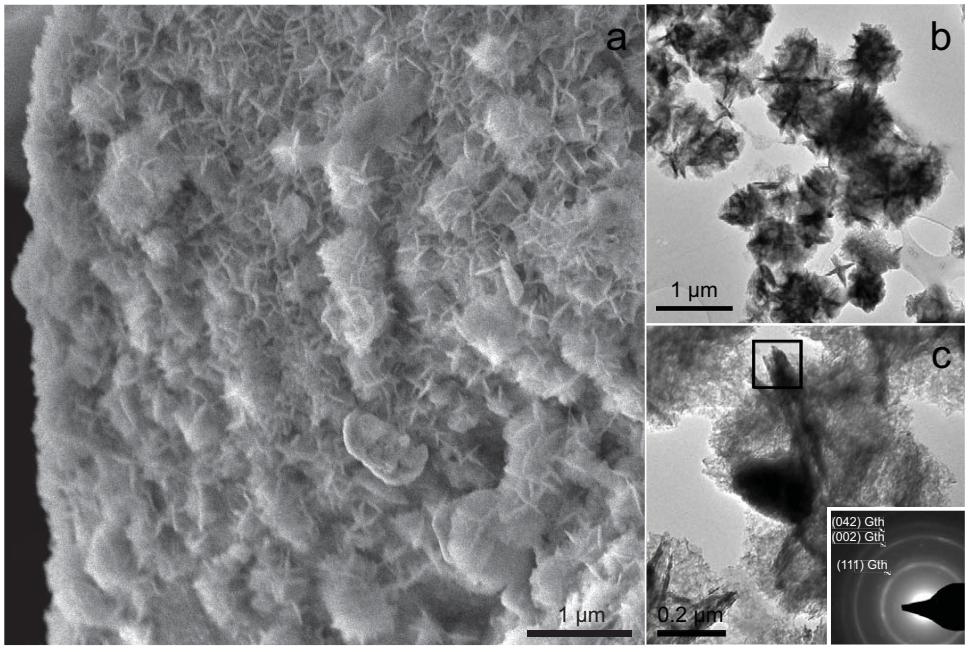

Figure 4. Needle aggregates of goethite. (a) SEM micrograph from CC-99-DBL-L (?fl). (b) TEM micrograph from CC-99-DBL-L. (c) TEM micrograph from BCC10 (nfl) with corresponding, indexed SAED pattern of the needle tip indicated in the boxed region, confirming that the needles are polycrystalline goethite (Gth).

can only form in slowly cooling plutonic environments [e.g., *Feinberg et al*., 2005], are particularly common. EDS analysis of individual lamellae was not possible due to limits on the spatial resolution of the electron beam's interaction volume; however, bulk EDS analyses indicated compositions with varying ratios of Ti and Fe. Low concentrations of ulvöspinel are not detectable in standard low-temperature MPMS experiments, as ulvöspinel is antiferromagnetic at room temperature, with a very weak ferromagnetic moment that appears at temperatures below 100 K [*Readman*, 1978].

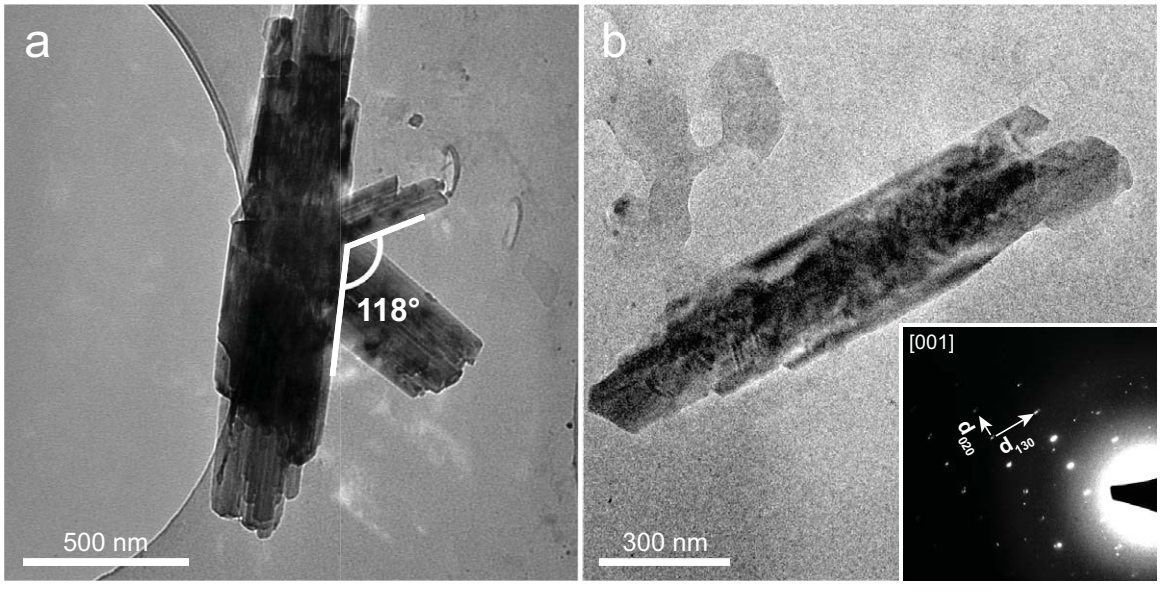

Figure 5. Solitary goethite needles, both from NC11-1 (fl). (a) TEM micrograph of twinned goethite needles with a twin angle of 118°. (b) TEM micrograph of a solitary goethite needle with SAED pattern along the [001] axis.

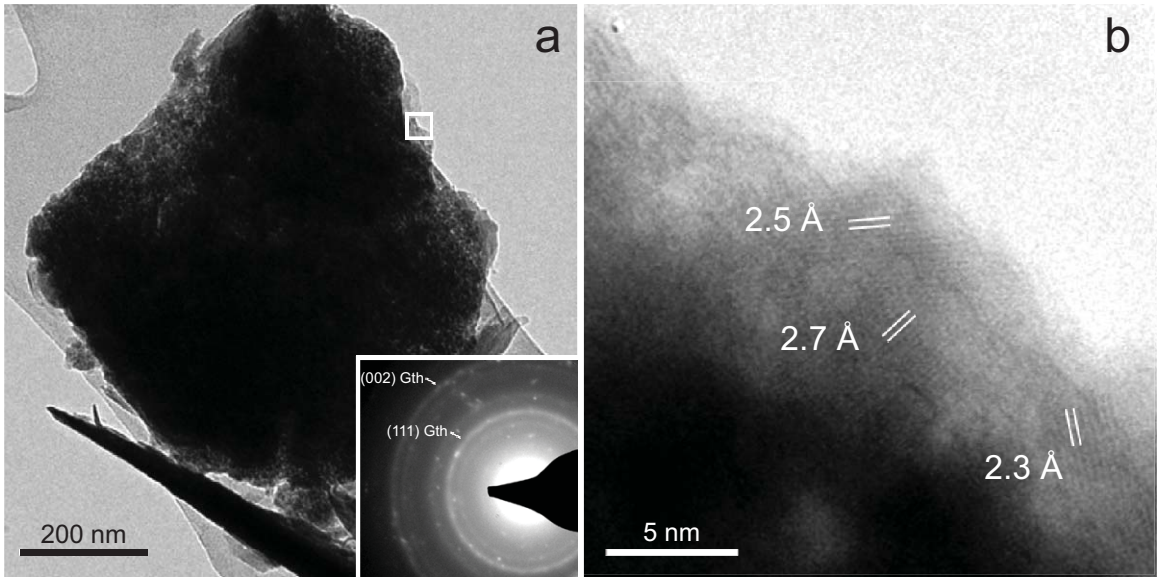

Figure 6. Polycrystalline aggregate of nanoscale goethite from SVC982 (fl). (a) TEM micrograph with inset polycrystalline SAED pattern. White box is the site of (b) HRTEM micrograph showing polycrystalline lattice fringes.

[49] Intergrowths of hematite (α-Fe_2O_3) and ilmenite ($FeTiO_3$) were observed in samples NC11-1 and SVC982 (Figures 7e–7f), with additional intergrowths of rutile (TiO_2) in the grain shown from NC11-1. Relict ilmenite lamellae display the lozenge shape characteristic of finely exsolved hematite-ilmenite systems, while hematite is largely etched away. Arrays of crystallographically aligned rutile inclusions crosscut both the ilmenite and hematite lamellae in the grain from NC11-1 shown in Figure 7f, consistent with exsolution in Ti-rich hemoilmenites [e.g., *Brownlee et al*., 2010]. As with the magnetite-ülvospinel intergrowths, EDS analysis of individual lamellae in these grains was not possible, though we may infer that these lamellae are composed of ilmenite and hematite, which is consistent with bulk EDS analysis of multiple sites on each grain showing various ratios of Fe and Ti. Magnetic experiments show no indication of hemoilmenite or its endmembers, hematite and ilmenite, indicating that the concentration of such exsolved grains in bulk samples is generally low. If these exsolved grains did contribute significantly to the remanence held by speleothems, extremely high coercivities would be expected. The exsolution process is known to transform large, formerly multidomain grains into populations of interacting single-domain grains [*Evans and Wayman*, 1974].

3.6. Spherules

[50] SEM examination of samples NC11-1, SVC982, and CC-99-DBL-L revealed at least one spherical grain with dendritic texture in each sample (Figure 8). Two of these spherules were identified through SEM-EDS analysis as titanomagnetite, with contributions from Cr, Ni, Na, and Si. These grains appear to be intergrown titanium oxide spheres with a less resistant matrix, consistent with the appearance of micrometeorites [e.g., *Onoue et al*., 2011], although they are at the low end of the range of typical spherule diameters, suggesting a possible categorization as cosmic dust.

3.7. Demagnetization of Remanent Magnetization

[51] Demagnetization of NRM in samples NC11-1, SVC982, CC-99-DBL-L, and BCC10 and isothermal remanent magnetization (IRM) in sample SVC06 (Figure 9) indicates that remanence is held by stalagmites in a variety of ways. Initial NRMs are reported in mass-normalized Am^2/kg, rather than volume-normalized units (e.g., A/m), due to the varying degrees of porosity in many stalagmites [*Frisia et al*., 2000]. Results in Zijderveld diagrams (Figure 9) are reported in Am^2, in order to give a clearer indication of how close a given sample is to the nominal sensitivity of the cryogenic magnetometer (10^{-12} Am^2).

[52] In samples NC11-1, SVC982, and CC-99-DBL-L, a single "soft" component of magnetization follows a trend generally toward the origin with the application of progressively larger alternating fields, though less directly in sample CC-99-DBL-L.

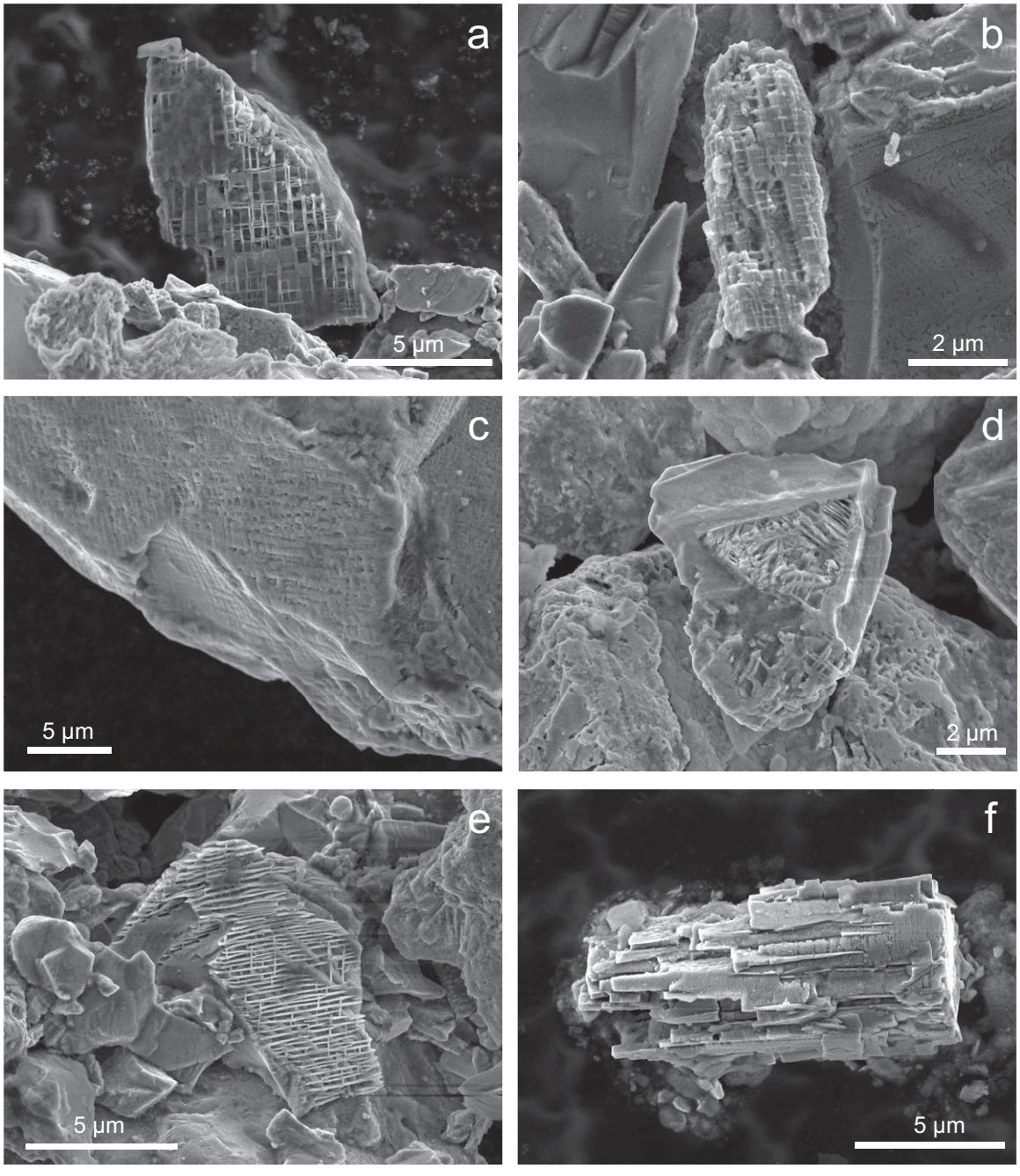

Figure 7. SEM images of grains exhibiting etched exsolution textures. Ulvöspinels from (a) SVC982 (fl), (b and c) NC11-1 (fl), (d) CC-99-DBL-L (?fl). (e) Hemoilmenite with rutile inclusions from NC11-1. (f) Hemoilmenite from SVC982.

Similarly, the progressive demagnetization of a 1 T IRM in sample SVC06 shows the near total removal of magnetic remanence after 170 mT, demonstrating the sample's capacity to record and hold a stable remanence. The extent of AF demagnetization suggests that magnetite and/or titanomagnetite are the major carriers of magnetic remanence in these four samples. In contrast, sample BCC10 shows a moderate mass-normalized NRM intensity but is resistant to AF demagnetization, suggesting that a significant portion of remanence in BCC10 is carried by a "hard" magnetic material. Based on both low-temperature magnetic results and electron microscopy, this material is likely goethite. It is unclear whether the goethite in BCC10 acquired a DRM at the time of stalagmite growth or acquired a

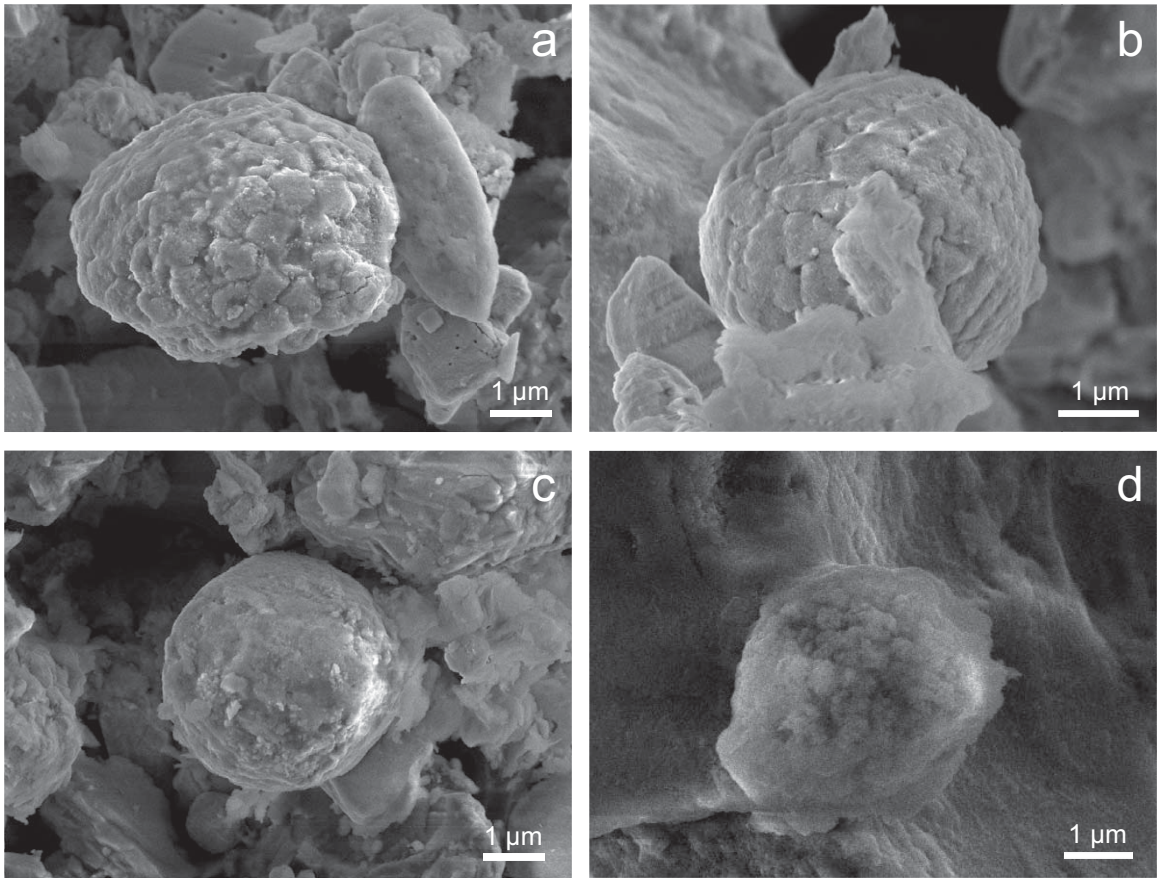

Figure 8. SEM images of spherules from (a) SVC982 (fl), (b) NC11-1 (fl), (c) SVC982, and (d) CC-99-DBL-L (?fl).

CRM over a protracted interval (see section 4.1); as such, the sample was treated with a 150°C thermal demagnetization step to remove any remanence held by goethite. However, the AF demagnetization spectra of BCC10 in Figure 9 illustrate one of the limitations on paleomagnetic studies of stalagmites: the residual remanence after thermal treatment falls near the noise level of the magnetometer and is too weak for the isolation of a characteristic remanent magnetization (ChRM). The remanence directions appear to cluster at a reasonable inclination given the location of the source cave, but the Zijderveld diagram demonstrates the noisy quality of the data.

4. Discussion

[53] *Perkins* [1996] divides magnetic extracts from speleothems into three categories: irregular and abraded grains, identified as detrital magnetite, titanomagnetite, and hematite; euhedral grains, identified as authigenic magnetite; and needle-shaped grains, identified as goethite. In fact, the results provided here demonstrate that the list of magnetic carriers in stalagmites is much more complex, and the previously established categories are overly broad. We replicate and expand upon Perkins's results with multiple lines of evidence—magnetic, chemical, and/or morphological—for each mineral identified as a source of remanence, including magnetite, titanomagnetite of varying compositions, goethite, and intergrown grains of ferromagnetic minerals.

[54] The diversity of magnetic minerals found is most fully represented in sample NC11-1, which includes detrital material of a high enough concentration and abundance to be visible at the hand sample scale. Other samples include a subset of the list, with varying contributions from each mineral. The remanence of samples NC11-1, SVC982, CC-99-DBL-L, and SVC06 is held primarily by magnetite and titanomagnetite. Only the remanence of sample BCC10 is dominated by goethite adequate to completely mask the Verwey transition during FC-ZFC experiments (Figure 1). While

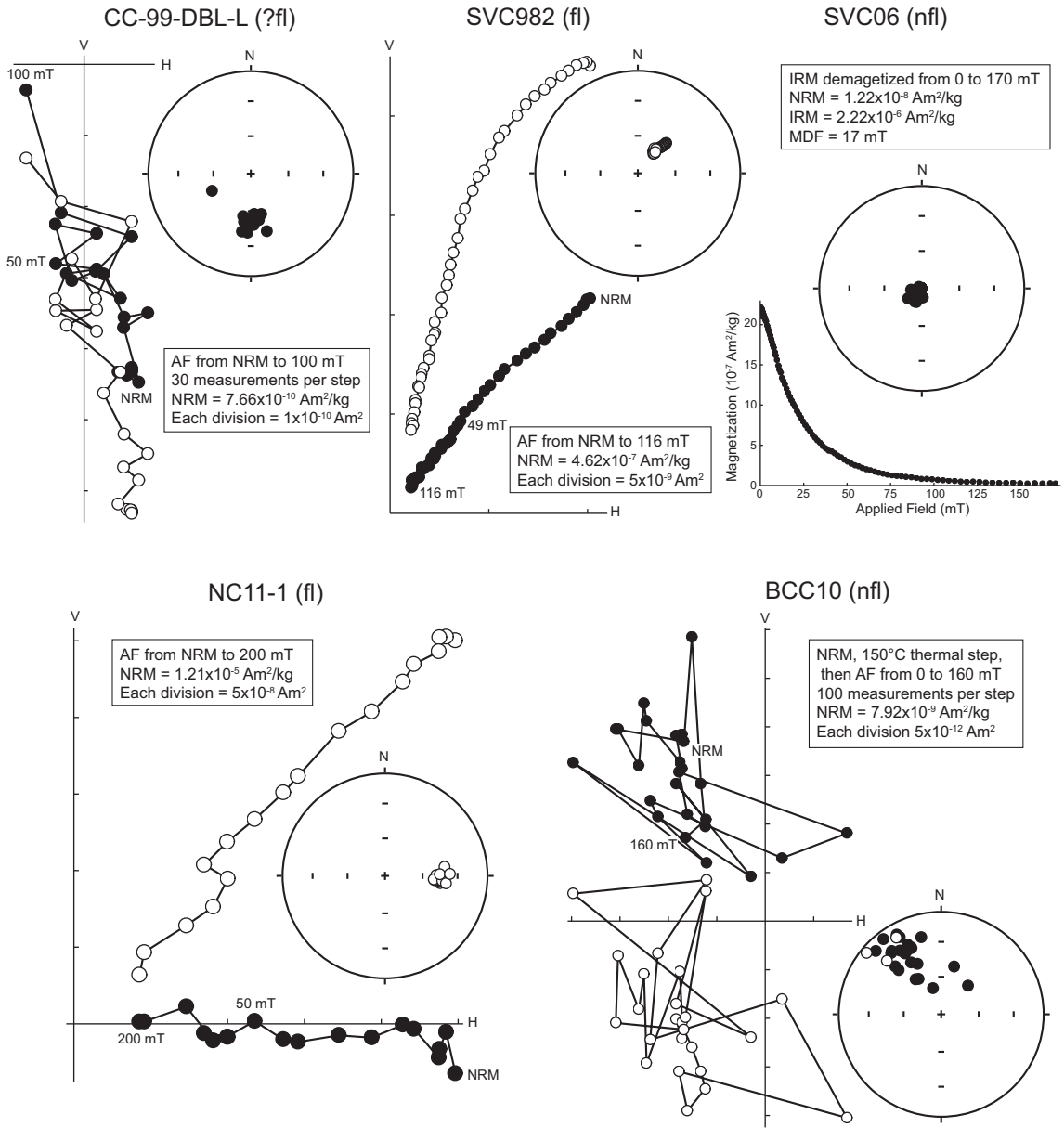

Figure 9. Representative Zijderveld plots and stereonets of the demagnetization of natural remanent magnetization (NRM) by sample, using either progressive alternating field (AF) or thermal steps. Unless otherwise noted, points represent a single measurement. Zijderveld plot omitted for sample SVC06 in favor of demagnetization of isothermal remanent magnetization (IRM) due to weakness of NRM. In Zijderveld plots, solid (hollow) circles represent horizontal (vertical) projection. In stereonets, solid (hollow) circles represent lower (upper) hemisphere. All samples in this figure are azimuthally unoriented.

ulvöspinel and hemoilmenite exsolution lamellae were detected microscopically, no contribution to magnetic remanence was observed.

[55] Other researchers [e.g., *Latham*, 1981; *Morinaga et al*., 1986; *Perkins and Maher*, 1993; *Perkins*, 1996; *Rusanov et al*., 2000; *Pruner et al*., 2010] have found evidence for hematite in speleothems through magnetic analyses. None of the five stalagmites used in this study indicated the presence of hematite through either magnetic or microscopic analysis (with the exception of intergrown hemoilmenite), though this does not preclude the possibility of hematite in other speleothems. Thermal demagnetization was not conducted on these speleothems, as goethite has been shown to be present and is known to convert to hematite after exposure to temperatures between 250°C and

400°C [*Dunlop and Özdemir*, 1997]. *Perkins* [1993] also posits the presence of maghemite, though he acknowledges that positive identification could not be made through his magnetic measurements. Similarly, *Latham et al*. [1989] did not rule out the possibility of maghemite in detrital matter. The observed shrinkage cracks along the surfaces of several magnetite and titanomagnetite grains in this study indicate that maghemite is likely present in some speleothems.

[56] Differential extraction from samples NC11-1, SVC982, and CC-99-DBL-L, which include flood layers (or, in the case of sample CC-99-DBL-L, are likely to have been exposed to flooding), yielded sufficiently large ($\geq$1 μm) magnetic grains to be examined through SEM in addition to a population of smaller grains studied through TEM. Samples SVC06 and BCC10, which show no evidence for flood layers, yielded no grains and smaller grains, respectively, suggesting a correlation between the presence of flood layers in stalagmites and a broader range of magnetic mineral grain sizes.

[57] Although no magnetite was positively identified in the single-domain (SD) size range through either TEM or SEM in any sample, magnetic results indicate the presence of magnetite in the SD through multidomain (MD) size range. In all FC-ZFC experiments performed, values in the FC warming curve were consistently higher than those in the ZFC warming curve at temperatures below 120 K, which indicates that all five samples are dominated primarily by SD and pseudosingle-domain (PSD) sized grains. The absence of SD magnetite in SEM and TEM imagery may be explained by a bias in the differential extraction method: any grains too weak to be attracted to the neodymium magnet or too small for this attraction to hold during agitation would not have been extracted for microscopic examination. This presented a particular problem for sample SVC06, which yielded no microscopically detectable magnetic material despite multiple extraction attempts. Sample SVC06 shows the limitation of the flask extraction method, which successfully isolated a magnetic extract for four out of five samples, but failed for a sample shown throughout magnetic experiments to contain trace concentrations of ferromagnetic material. Additional work is necessary to improve the method and address this issue.

[58] Samples SVC982 and SVC06, which were collected from the same cave system, exemplify the dichotomy between stalagmites with and without flood layers. One might expect that samples without flood layers should display lower NRM and IRM intensities than those with flood layers; this trend does not hold in low-temperature FC-ZFC experiments, during which sample SVC982 (with flood layers) retains remanence less readily than sample SVC06 (without flood layers). This may be explained by magnetic grain size: if sample SVC982 includes magnetic material that is MD in size, in accordance with the proposed relationship between magnetic grain size and flood material, its remanence should be less stable than that of sample SVC06, which includes smaller SD magnetic grains. The magnetic dichotomy is consistent with SEM and TEM observations indicating a much broader range of grain sizes, especially larger grains, in sample SVC982 relative to sample SVC06. The contrast between these two samples from a single cave indicates that the information gained from a single speleothem may not fully describe its depositional environment, especially with respect to its source waters and catchment basin.

[59] In all samples analyzed via SEM (NC11-1, SVC982, CC-99-DBL-L), grain morphologies ranged from perfectly euhedral (especially in the case of magnetite and titanomagnetite) to extensively pitted to heavily fractured and abraded, all within a single subsample. This variation suggests that magnetic material follows multiple routes of transport into a cave system prior to deposition and encapsulation on a stalagmite's drip surface. While some grains were pitted, most were not, indicating that a subset of the magnetic grains had been subject to chemical weathering prior to their incorporation into these stalagmite samples. The broad range of physical abrasion in grains of similar dimensions may indicate that detrital magnetic material has been sourced from varying distances and undergone multiple types of transport.

4.1. The Source of CRM

[60] The crystallographic habit of the goethite identified through diffraction and elemental analysis in this study is distinct from that of the grains suggested to be goethite in *Perkins* [1996], which were identified by morphology alone. Our three goethite subcategories (needle aggregates, solitary needles, and polycrystalline aggregates) are differentiated by morphology, a commonly used proxy for transport history. We infer that the polycrystalline aggregate grains are the product of rapid nucleation, with little particle growth, whereas the needle-shaped grains result from slower nucleation

and increased particle growth. However, the specific conditions that give rise to these habits are currently unknown, and in the absence of additional data, we cannot conclusively determine whether the goethite formed prior to reaching the cave environment or precipitated inside the cave. A better understanding of the mechanisms behind the introduction of goethite to cave systems may provide useful insight into the origins of the varied morphologies observed in this study, as well as their role in remanence acquisition and potential use as a proxy for environmental conditions.

[61] While it is currently impossible to prove that goethite formed authigenically on the surface of these particular stalagmites, we propose that the precipitation of goethite is favorable in most cave environments. Drip waters in most karst environments, excluding those characterized by sulfidic groundwater, have pH values ranging from 7 to 8 and Eh values ranging from 0.4 V to 0.6 V [*White*, 1997]. When groundwater is first exposed to the atmosphere inside a cave, dissolved CO_2 outgasses from the drip water, causing its pH to gradually increase and reducing the solubility of dissolved iron, which leads to the precipitation of iron-bearing minerals [*Dreybrodt*, 2012]. According to the Eh-pH phase diagram of *Lemos et al*. [2007] showing the thermodynamic stability fields of various iron minerals, most drip waters fall decisively within the stability field of goethite. In contrast, stability conditions for magnetite require significantly lower pH values and corresponding Eh values below 0.0 V, and the thermodynamic environment of most groundwater is far from favorable to these conditions. In fact, iron-sulfide minerals such as pyrite and pyrrhotite would precipitate from cave drip water before magnetite became thermodynamically favorable. While abiotic precipitation of magnetite is unlikely, it is possible that magnetite could be produced in situ on stalagmite surfaces if local Eh-pH conditions were biologically mediated on the submillimeter scale, an idea first proposed by *Perkins and Maher* [1993].

[62] Regardless of where goethite forms, either authigenically on a stalagmite surface or immediately adjacent to a cave system, the combination of goethite's submicron grain size and exceedingly low saturation magnetization (0.31 ± 0.03 $Am^2 kg^{-1}$) [*Martin-Hernandez and García-Hernández*, 2010] make it unlikely that such grains would be able to overcome the Brownian motion of water molecules in order to rotate into statistical alignment with the Earth's magnetic field and acquire a depositional remanent magnetization (DRM) [*Tauxe*, 2013]. The different morphologies of goethite observed in this study suggest that factors like water chemistry, ambient temperature, and drip rate may play important roles in determining the particular morphology of goethite that is hosted by a stalagmite. This remains an active area of research, but unless it can be demonstrated that magnetite can precipitate directly in a cave environment, any chemical remanent magnetizations (CRMs) held by speleothems are most likely held by goethite. However, as it has not yet been conclusively shown that goethite precipitates concurrently with its host calcite layer in a stalagmite, we caution against reliance on this component, especially in light of concerns about the effects of post-depositional CRMs in sediment cores [*Lascu and Feinberg*, 2011].

4.2. The Source of DRM

[63] The speleothems addressed in this study that are best suited for rock magnetic analyses have elevated NRM intensities due to the presence of detrital magnetite and titanomagnetite. The titanomagnetite, exsolved ulvöspinel, and exsolved hemoilmenite grains imaged in samples NC11-1, SVC982, and CC-99-DBL-L could not have formed inside the cave environment; these minerals form exclusively in igneous environments, and the exsolution textures observed on several grains form only during slow cooling of igneous intrusions. Likewise, the titanium content of the spherules found in these three caves precludes their formation in the caves or their overlying soils, suggesting that they originated from micrometeorites or volcanic eruptions. (The spherules also share a similar appearance to industrial fly-ash, yet this origin can be excluded as all samples examined in this study significantly predate the onset of the Industrial Revolution.) Further, Niagara Cave, Spring Valley Caverns, and Crevice Cave are all situated to the south of their respective nearest igneous intrusions. These grains must therefore be allochthonous in origin and the remanence they carry is categorized as depositional remanent magnetization (DRM). However, these grains are not always heavily abraded, as would be expected in the morphological model put forward by *Perkins* [1996]; in fact, fine lamellae are readily visible on multiple grains through SEM (Figures 7a–7e). Rather, this study indicates that there is not likely to be a single specific grain morphology associated with the magnetic minerals that carry a stalagmite's DRM.

[64] We suggest that glaciers moving north to south may have played a role in the transport of these grains from intrusion to cave flood source region, either through primary transport by the ice itself or secondary transport by outwash. Although none of these caves were covered with glaciers during the most recent glacial maximum, outwash from earlier glacial melt could have carried these grains further south. The small size of the allochthonous grains (<5 μm) would allow them to be suspended within downward percolating groundwaters and ultimately deposited as magnetic detritus within cave drip water.

[65] *Latham et al*. [1989] studied magnetic extracts from speleothems, using light microscopy to detect both magnetite and titanomagnetite, which was indicated by exsolution lamellae. *Perkins* [1996] does not report any exsolved grains. This study is the first (of which we are aware) to report both exsolved exsolution textures and elemental analyses for these types of grains in speleothems.

4.3. The Combined Application of Rock Magnetism and Electron Microscopy

[66] The combined rock magnetic and electron microscopy methods used in this study allow for a more nuanced understanding of the magnetic mineral assemblage found in speleothems. Rock magnetic characterization suggests that magnetite, titanomagnetite, and goethite are the primary paleomagnetic recorders in these five stalagmites. However, microscopy reveals that this analysis does not tell the entire story. Multiple ulvöspinel and hemoilmenite grains were identified microscopically, with no indication from magnetic results, providing otherwise unobtainable information about the transport history of magnetic material in these stalagmites. Further, the multiple morphologies of goethite indicate several subpopulations of grains, each of which formed in a unique thermodynamic environment, which would have been impossible to determine from magnetic study alone.

[67] Even speleothems with low magnetic intensity, as indicated by saturation magnetization (Ms), are potentially rewarding for magnetic extraction and microscopy. The Ms of sample CC-99-DBL-L is the lowest of all five samples; however, differential extraction yielded a population of magnetic grains spanning the size ranges appropriate for both SEM and TEM analysis. In contrast, the Ms of sample SVC06 is a full order of magnitude higher, but this sample yielded inadequate magnetic extracts for microscopic analysis. Further refinement and testing of the differential extraction method is necessary.

4.4. Further Work and Applications

[68] There remains a great deal to be discovered regarding the magnetic minerals in speleothems. Future expansion of this study would enlarge the range of factors considered to include the chemistry of the cave environment, sample collection depth, and the influence of geographic factors like proximity to igneous provinces and exposure to glacial events. The determination of potential biological influences on the magnetic mineral assemblage in speleothems is of particular importance, as it may enable researchers to determine conclusively whether magnetite can precipitate in situ on a stalagmite surface. Further analysis of the conditions necessary for the precipitation of goethite in cave systems may elucidate the utility of speleothems for environmental magnetism. With a better understanding of the roles of environmental indicators like Eh and pH, goethite growth could be used as a proxy for climatic conditions, complementing current paleoclimate research based on carbon and oxygen isotopic ratios in speleothems, especially with respect to compositional changes in wet and dry periods that covary with environmental conditions.

[69] The ubiquitous presence of goethite in our stalagmite samples suggests that care should be taken in rock magnetic studies to remove any unwanted chemical remanence associated with this mineral. We suggest a thermal pretreatment step of 150°C in zero field. The Néel temperature of goethite ranges from 102°C for large, defect-poor single crystals to ~120°C for poorly crystalline samples with high concentrations of mineral defects [*Martin-Hernandez and García-Hernández*, 2010]; therefore, pretreatment at 150°C should provide adequate thermal energy to remove all goethite remanence. This thermal step may also remove a portion of the low-coercivity remanence held by magnetite and titanomagnetite, reducing the overall remanence to an intensity near the sensitivity limit of most SQUID-based cryogenic rock magnetometers, but it will improve the likelihood that the remaining remanence is held by detrital grains. The remaining remanence can then be quantified using traditional alternating field methods for samples dominated by low-coercivity magnetic minerals, such as magnetite and titanomagnetite and their partially oxidized equivalents, or thermal

demagnetization for samples dominated by high-coercivity magnetic minerals, such as hematite.

5. Concluding Remarks

[70] The combined rock magnetic and electron microscopic analysis of five North American stalagmites proved to be a useful method in describing the correlation between paleomagnetic remanence and magnetic mineral assemblages. In all samples, magnetite and goethite were present in varying abundances and morphologies. Magnetite grains displayed features characteristic of transport, including plumose markings and etch pits, providing evidence of a detrital origin. Titanomagnetite and exsolved intergrowths of iron-titanium oxides were also found through microscopic analysis, further emphasizing that a significant portion of the magnetic mineral assemblage is allochthonous and must have been transported over a considerable distance to reach the cave system. The allochthonous grains display a range of morphologies, from euhedral to well rounded, suggesting that the morphological model of *Perkins* [1996] does not apply fully in every geologic setting. These detrital grains likely hold a depositional remanent magnetization, whereas the goethite grains observed are unlikely to hold a depositional remanence due to their small size and low saturation magnetization. If they were precipitated in situ on the stalagmite's drip surface, they may instead hold a chemical remanent magnetization. Further study is needed to determine the paleomagnetic significance of goethite remanence; until then, we suggest that paleomagnetic studies of stalagmites include a 150°C thermal demagnetization step in order to remove any remanence held by goethite.

Acknowledgments

[71] We are grateful to E.C. Alexander Jr. and R.L. Edwards for providing samples, and to John Ackerman and the Minnesota Cave Preserve for providing access to Spring Valley Cavern. Harry Rowe and Greg Springer facilitated access to samples from Buckeye Creek Cave. Mike Jackson and the staff of the IRM graciously provided technical input and guidance. Comments by David Heslop and two anonymous reviewers greatly improved the manuscript. This research was supported by NSF grant EAR-1316385 to J. M. F., a Ralph W. Stone graduate fellowship from the National Speleological Society to B. E. S., and NSF grant ECS-1012193 to J.H.S. Parts of this work were carried out in the Characterization Facility, University of Minnesota, a member of the NSF-funded Materials Research Facilities Network (www.mrfn.org) via the MRSEC program. Magnetic measurements were conducted at the Institute for Rock Magnetism, University of Minnesota. This is IRM publication 1307.

References

Brownlee, S. J., J. M. Feinberg, R. J. Harrison, T. Kasama, G. R. Scott, and P. R. Renne (2010), Thermal modification of hematite-ilmenite intergrowths in the Ecstall pluton, British Columbia, Canada, *Am. Mineral.*, *95*, 153–160, doi: 10.2138/am.2010.3191.

Cornell, R. M., and U. Schwertmann (2003), *The Iron Oxides*, 2nd ed., pp. 71, John Wiley, Weinheim, Germany.

Dasgupta, S. (2008), High-resolution speleothem record of late Quaternary climate change from the Upper Midwest, USA, PhD thesis, Dep. of Geology, Univ. of Minn., Minneapolis, Minn.

Denniston, R. F., Y. Asmerom, V. Polyak, J. A. Dorale, S. J. Carpenter, C. Trodick, B. Hoye, and L. A. González (2007), Synchronous millennial-scale climatic changes in the Great Basin and the North Atlantic during the last interglacial, *Geology*, *35*, 619–622, doi:10.1130/G23445A.1.

Dorale, J. A., R. L. Edwards, E. Ito, and L. A. González (1998), Climate and vegetation history of the Midcontinent from 75 to 25 ka: A speleothem record from Crevice Cave, Missouri, USA, *Science*, *282*, 1871–1874, doi:10.1126/science.282.5395.1871.

Dorale, J. A., R. L. Edwards, E. C. Alexander Jr., C.-C. Shen, D. A. Richards, and H. Cheng (2004), Uranium-series dating of speleothems: Current techniques, limits, & applications, in *Studies of Cave Sediments: Physical and Chemical Records of Paleoclimate*, edited by I. R. Sasowsky and J. Mylroie, pp. 177–197, Springer, Dordrecht, Netherlands.

Dreybrodt, W. (2012), Caveat: Pitfalls in the measurement of pH of drip waters in caves, *Acta Carsol.*, *41*, 157–160.

Dunlop, D. J., and Ö. Özdemir (1997), *Rock Magnetism: Fundamentals and Frontiers*, Cambridge Univ. Press, Cambridge, U. K.

Evans, M. E., and M. L. Wayman (1974), An investigation of the role of ultra-fine titanomagnetite intergrowths in palaeomagnetism, *Geophys. J. R. Astron. Soc.*, *33*, 1–10, doi: 10.1111/j.1365-246X.1974.tb03621.x.

Fairchild, I. J., S. Frisia, A. Borsato, and A. F. Tooth (2007), Speleothems, in *Geochemical Sediments and Landscapes*, edited by D. J. Nash and S. J. McLaren, pp. 200–245, Blackwell, Oxford, U. K.

Feinberg, J. M., G. R. Scott, P. R. Renne, and H.-R. Wenk (2005), Exsolved magnetite inclusions in silicates: Features determining their remanence behavior, *Geology*, *33*, 513–516, doi:10.1130/G21290.1.

Frisia, S., A. Borsato, I. J. Fairchild, and F. McDermott (2000), Calcite fabrics, growth mechanisms, and environments of formation in speleothems from the Italian Alps and southwestern Ireland, *J. Sediment. Res.*, *70*, 1183–1196, doi: 10.1306/022900701183.

Hardt, B. F. (2010), Changes in seasonal precipitation of East Central North America with Connections to Global Climate, PhD thesis, Dep. of Geology, Univ. of Minn., Minneapolis, Minn.

Lascu, I., and J. M. Feinberg (2011), Speleothem magnetism, *Quat. Sci. Rev.*, *30*, 3306–3320, doi:10.1016/j.quascirev.2011.08.004.

Latham, A. G. (1981), Paleomagnetism, rock magnetism and U-Th dating of speleothem deposits, PhD thesis, Dep. of Geology, McMaster Univ., Hamilton, Ontario, Canada.

Latham, A. G., H. P. Schwarcz, D. C. Ford, and G. W. Pearce (1979), Paleomagnetism of stalagmite deposits, *Nature*, *280*, 383–385, doi:10.1038/280383a0.

Latham, A., H. P. Schwarcz, D. C. Ford, and G. W. Pearce (1982), The paleomagnetism and U-Th dating of three Canadian speleothems: Evidence for the westward drift, 5.4–2.1 ka BP, *Can. J. Earth Sci.*, *19*, 1985–1995, doi:10.1139/e82-176.

Latham, A. G., H. P. Schwarcz, and D. C. Ford (1986), The paleomagnetism and U-Th dating of Mexican stalagmite, DAS2, *Earth Planet. Sci. Lett.*, *79*, 195–207, doi:10.1016/0012-821X(86)90053-1.

Latham, A. G., D. C. Ford, H. P. Schwarcz, and T. Birchall (1989), Secular variation from Mexican stalagmites: Their potential and problems, *Phys. Earth Planet. Inter.*, *56*, 34–48, doi:10.1016/0031-9201(89)90034-4.

Lemos, V. P., M. Lima da Costa, R. L. Lemos, and M. S. Gomes de Faria (2007), Vivianite and siderite in lateritic iron crust: An example of bioreduction, *Quim. Nova*, *30*, 36–40, doi:10.1590/S0100-40422007000100008.

Martin-Hernandez, F., and M. M. García-Hernández (2010), Magnetic properties and anisotropy constant of goethite single crystals at saturating high fields, *Geophys. J. Int.*, *181*, 756–761, doi:10.1111/j.1365-246X.2010.04566.x.

Morinaga, H., H. Inokuchi, and K. Yaskawa (1986), Magnetization of a stalagmite in Akiyoshi Plateau as a record of the geomagnetic secular variation in West Japan, *J. Geomagn. Geoelectr.*, *38*, 27–44, doi:10.5636/jgg.38.27.

Morinaga, H., M. Kamino, H., Inokuchi, and K. Yaskawa (1987), Remanent magnetization of synthetic stalagmites, *Rock Magn. Paleogeophys.*, *14*, 13–17.

Morinaga, H., I. Horie, and K. Yaskawa (1992), A geomagnetic reversal recorded in a stalagmite collected in western Japan, *J. Geomagn. Geoelectr.*, *44*, 661–675, doi:10.5636/jgg.44.661.

Moskowitz, B. M., M. Jackson, and C. Kissel (1998), Low-temperature magnetic behavior of titanomagnetites, *Earth Planet. Sci. Lett.*, *157*, 141–149, doi:10.1016/S0012-821X(98)00033-8.

Onoue, T., T. Nakamura, T. Haranosono, and C. Yasuda (2011), Composition and accretion rate of fossil micrometeorites recovered in Middle Triassic deep-sea deposits, *Geology*, *39*, 567–570, doi:10.1130/G31866.1.

Openshaw, S., A. Latham, and J. Shaw (1997), Speleothem paleosecular variation records from China: Their contribution to the coverage of Holocene paleosecular variation data in East Asia, *J. Geomagn. Geoelectr.*, *49*, 485–505, doi:10.5636/jgg.49.485.

Osete, M.-L., J. Martín-Chivelet, C. Rossi, R. L. Edwards, R. Egli, M. B. Muñoz-García, X. Wang, F. J. Pavón-Carrasco, and F. Heller (2012), The Blake geomagnetic excursion recorded in a radiometrically dated speleothem, *Earth Planet. Sci. Lett.*, *353–354*, 173–181, doi:10.1016/j.epsl.2012.07.041.

Oster, J. L., I. P. Montañez, T. P. Guilderson, W. D. Sharp, and J. L. Banner (2010), Modeling speleothem $\delta^{13}C$ variability in a central Sierra Nevada cave using ^{14}C and $^{87}Sr/^{86}Sr$, *Geochim. Cosmochim. Acta*, *74*, 5228–5242, doi:10.1016/j.gca.2010.06.030.

Perkins, A. M. (1993), Magnetic studies of speleothems, PhD thesis, Univ. of East Anglia, Norwich, U. K.

Perkins, A. M. (1996), Observations under electron microscopy of magnetic minerals extracted from speleothems, *Earth Planet. Sci. Lett.*, *139*, 281–289, doi:10.1016/0012-821X(96)00013-1.

Perkins, A. M., and B. A. Maher (1993), Rock magnetic and paleomagnetic studies of British speleothems, *J. Geomagn. Geoelectr.*, *45*, 243–153, doi:10.5636/jgg.45.143.

Pruner, P., N. Z. Hajna, A. Mihevc, P. Bosák, O. Man, P. Schnabl, and D. Venhodová (2010), Magnetostratigraphy and fold tests from Račiška pečina and Pečina v Borštu caves (Classical Karst, Slovenia), *Stud. Geophys. Geod.*, *54*, 27–48, doi:10.1007/s11200-010-0002-1.

Readman, R. W. (1978), Magnetic properties of ulvöspinel, *Phys. Earth Planet. Inter.*, *16*, 196–199, doi:10.1016/0031-9201(78)90011-0.

Rusanov, V., R. G. Gilson, A. Lougear, and A. X. Trautwein (2000), Mössbauer, magnetic, X-ray fluorescence and transmission electron microscopy study of natural magnetic materials from speleothems: Haematite and the Morin transition, *Hyperfine Interact.*, *128*, 353–373, doi:10.1023/A:1012668623559.

Shapiro, D. (2007), Evidence for wide scale climate forcing in the late Pleistocene from a speleothem stable isotope record from Spring Valley Caverns, Fillmore Country, Minnesota, Bachelor's thesis, Carleton College, Northfield, Minn.

Tauxe, L. (2013), *Essentials of Paleomagnetism*, 2nd Web ed., [Available at http://magician/ucsd.edu/Essentials_2.].

Thermo Electron Corporation (2009), *NORAN System SIX, Model 300 User's Handbook*, pp. *217*, Madison, Wisconsin.

Vacco, D. A., P. U. Clark, A. C. Mix, H. Cheng, and R. L. Edwards (2005), A speleothem record of Younger Dryas cooling, Klamath Mountains, Oregon, USA, *Quat. Res.*, *64*, 249–256, doi:10.1016/j.yqres.2005.06.008.

White, W. B. (1997), Thermodynamic equilibrium, kinetics, activation barriers, and reaction mechanisms for chemical reactions in Karst Terrains, *Environ. Geol.*, *30*, 46–58, doi:10.1007/s002540050131.

Whitney, D. L., and B. W. Evans (2010), Abbreviations for names of rock-forming minerals, *Am. Mineral.*, *95*, 185–187, doi:10.2138/am.2010.3371.